Journal of Solid State Chemistry 181 (2008) 1582–1589

Contents lists available at ScienceDirect

Journal of Solid State Chemistry

journal homepage: www.elsevier.com/locate/jssc

Luminescence in colloidal Mn^{2+}-doped semiconductor nanocrystals

Rémi Beaulac, Paul I. Archer, Daniel R. Gamelin *

Department of Chemistry, University of Washington, Seattle, WA 98195, USA

ARTICLE INFO

Article history:
Received 12 March 2008
Received in revised form
24 April 2008
Accepted 3 May 2008
Available online 9 May 2008

Keywords:
Nanocrystals
Colloids
Luminescence spectroscopy
Mn^{2+}
Diluted magnetic semiconductors
Quantum dots

ABSTRACT

Recent advances in nanocrystal doping chemistries have substantially broadened the variety of photophysical properties that can be observed in colloidal Mn^{2+}-doped semiconductor nanocrystals. A brief overview is provided, focusing on Mn^{2+}-doped II–VI semiconductor nanocrystals prepared by direct chemical synthesis and capped with coordinating surface ligands. These Mn^{2+}-doped semiconductor nanocrystals are organized into three major groups according to the location of various Mn^{2+}-related excited states relative to the energy gap of the host semiconductor nanocrystals. The positioning of these excited states gives rise to three distinct relaxation scenarios following photoexcitation. A brief outlook on future research directions is provided.

1. Introduction

Colloidal doped semiconductor nanocrystals (doped quantum dots) have drawn considerable attention in recent years. Such materials have been shown to display efficient sensitized impurity luminescence [1–11], large magneto-optical effects [7,12–16], and interesting quantum size effects on impurity-carrier binding energies [17]. They have been proposed for use as biological labels [2,18,19] and as recombination centers in hybrid organic/inorganic electroluminescent devices [20,21]. They could potentially even find application as spin filters in future spin-based information processing devices [22,23]. Dopants within nanocrystals have been used as probes of microscopic structural parameters, [24–26] and charged/doped colloidal nanocrystals have been examined experimentally [27] and theoretically [23,28–31] as models for magnetic polarons. Colloidal doped oxide semiconductor nanocrystals have played an important role in revealing the significance of grain-boundary defects in activating the high-temperature ferromagnetism sometimes observed in these materials [13,32–37]. The synthetic challenges of doping semiconductor nanocrystals have also provided fertile grounds for investigation of the basic chemistries of homogeneous nucleation and crystal growth in the presence of impurities [38]. Dopant exclusion from critical nuclei has been suggested to be a general phenomenon [13,15,38,39], and the modes of dopant binding to crystallite surfaces have been investigated experimentally [40] and theoretically [41] in the context of impurity incorporation. For related reviews containing more description of sample syntheses, the reader is referred to Refs. [1–3,38,42] and references therein.

This short review focuses on one of the most fundamental physical properties of colloidal doped semiconductor nanocrystals, namely the nanocrystal photoluminescence (PL). The discussion focuses on Mn^{2+} as a dopant, and on II–VI semiconductors as hosts. Although the luminescence of doped semiconductors has attracted a great deal of interest for many years, the emergence of synthetic methodologies for preparing high-quality colloidal doped semiconductor nanocrystals has sparked renewed interest in this class of materials. Even within the narrow range of materials covered in this review (Mn^{2+}-doped II–VI semiconductor nanocrystals), a rich variety of photophysical properties is already found, and large qualitative changes in these physical properties (and hence in potential applications) can be achieved through changes in the host semiconductor lattice or through quantum confinement effects. This wealth of physical properties is attractive for future applications of such materials.

2. Case studies of luminescence in Mn^{2+}-doped II–VI semiconductor nanocrystals

In this section, Mn^{2+}-doped II–VI semiconductor nanocrystals are organized into three distinct categories according to the nature of their lowest energy excited state, which determines their resulting photophysical properties.

* Corresponding author. Fax: +1 206 685 8665.
E-mail address: Gamelin@chem.washington.edu (D.R. Gamelin).

0022-4596/$ - see front matter © 2008 Elsevier Inc. All rights reserved.
doi:10.1016/j.jssc.2008.05.001

2.1. Scenario I: Mn^{2+} ligand-field excited states are lowest in energy and within the gap

The most commonly studied group of Mn^{2+}-doped semiconductor nanocrystals are those in which the Mn^{2+} ligand-field excited states reside within the optical gap of the host semiconductor. Examples include Mn^{2+}-doped ZnS, ZnSe, and CdS nanocrystals [4,6,7,9,10,12,19].

For both octahedral and tetrahedral weak-field geometries, the ground state of Mn^{2+} is $^6A_1$ (Fig. 1). The first ligand-field excited state is $^4T_1$ derived from the ^4G free ion term. To higher energies, a large number of quartet ($^4\Gamma$) and doublet ($^2\Gamma$) states provide a near-continuous density of states. Transitions from the $^6A_1$ ground state to all of these ligand-field excited states are spin forbidden and gain only slight allowedness through spin–orbit coupling. Consequently, absorption transitions such as $^6A_1 \rightarrow {}^4T_1$ have molar extinction coefficients of $\varepsilon_{Mn^{2+}} \sim 10^0$–$10^1\,M^{-1}\,cm^{-1}$ at their maxima [43], compared with $\varepsilon_{QD} \sim 10^5$–$10^6\,M^{-1}\,cm^{-1}$ for the first absorption maximum of a typical semiconductor quantum dot [44,45]. This spin forbiddenness also leads to small radiative rate constants for the $^4T_1 \rightarrow {}^6A_1$ luminescence transition (arrow in Fig. 1), but the large $^4T_1$–$^6A_1$ energy gap combined with the low phonon energies provided by most II–VI semiconductor lattices still allows for $^4T_1 \rightarrow {}^6A_1$ PL with high quantum efficiencies. This is the transition most commonly described in PL studies of Mn^{2+}-doped semiconductor nanocrystals.

Fig. 2 shows representative room-temperature PL data collected in the Meijerink laboratories for a series of hexadecylamine-capped Mn^{2+}-doped ZnSe (cubic) nanocrystals with various Mn^{2+} concentrations [4]. As Mn^{2+} is added, the excitonic luminescence intensity at $\sim$23,500 cm^{-1} is quenched, and a new luminescence feature centered at $\sim$17,300 cm^{-1} appears. This new luminescence feature is the spin-forbidden $^4T_1 \rightarrow {}^6A_1$ ligand-field transition (Fig. 1). Above the $^4T_1$ excited state, the series of distorted ligand-field excited states (Fig. 1) ensure that the conditions for energy-conserving semiconductor-to-Mn^{2+} energy transfer (described by $k_{ET}^{Mn^{2+}}$ in Fig. 2) may generally be met. From these upper excited ligand-field states, internal relaxation to the

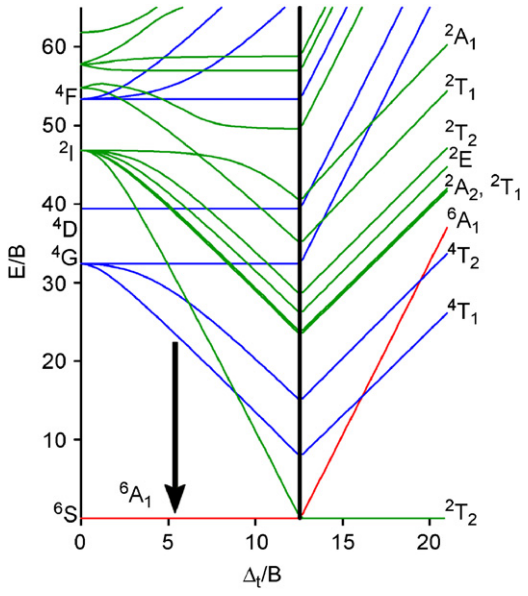

Fig. 1. Energy level diagram for Mn^{2+} (d^5) in a cubic geometry calculated from the Tanabe–Sugano matrices, showing several spin-forbidden ligand-field excited states, and indicating the emissive $^4T_1 \rightarrow {}^6A_1$ ligand-field transition observed in Mn^{2+}-doped ZnS and many other Mn^{2+}-doped II–VI semiconductor nanocrystals. Energies calculated for $C/B = 4.48$.

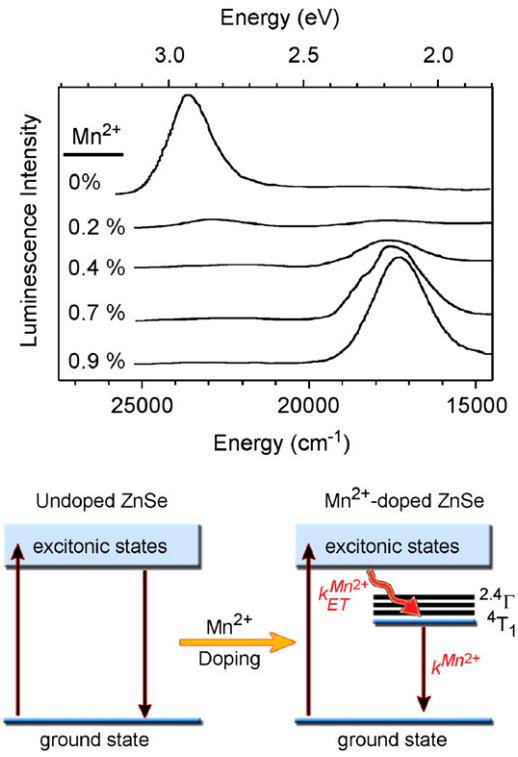

Fig. 2. Room-temperature photoluminescence spectra of Mn^{2+}:ZnSe nanocrystals with various concentrations of Mn^{2+} between 0.2 and 0.9 cation mole percent. As Mn^{2+} is introduced, exciton quenching via energy transfer to Mn^{2+} is observed, as summarized schematically below. Data adapted from Ref. [4].

$^4T_1$ state proceeds rapidly via phonon emission. The large energy gap between the $^4T_1$ excited state and the ground state contributes to the high PL quantum yields and nearly radiative excited state lifetimes that can be achieved in Mn^{2+}-doped nanocrystals of this type. In Mn^{2+}-doped ZnS nanocrystals, for example, slow single-exponential decay with a very long lifetime ($\tau = 1.9$ ms at 300 K, Ref. [6]) comparable to that of bulk Mn^{2+}:ZnS ($\tau = 1.8$ ms at 4.2 K and above [46]) has been reported for isolated Mn^{2+} ions within the nanocrystal lattices. Shorter Mn^{2+} PL lifetimes arising from Mn^{2+}–Mn^{2+} exchange interactions are generally observed, and some groups have also reported a fast Mn^{2+} PL decay associated with surface-exposed Mn^{2+} ions [47,48].

Energy transfer to the Mn^{2+} is too fast to have been resolved in the nanosecond pump-probe experiments on the samples of Fig. 2, indicating that $k_{ET}^{Mn^{2+}}$ must be comparable to or larger than the ZnSe radiative decay rate constants. Picosecond exciton quenching can be inferred from experiments on self-assembled QDs grown by molecular beam epitaxy [49]. The most efficient energy transfer processes in these nanocrystals most likely involve exchange interactions similar to those described by Dexter for sensitization of luminescence in doped insulating lattices [50]. The high efficiency of exchange-based mechanisms in doped QDs can be attributed to spatial confinement of the exciton in the same locale as the dopants. In uniformly doped nanocrystals, this invariably leads to almost complete quenching of the excitonic emission, such as observed in the Mn^{2+}:ZnSe QDs of Fig. 2. By the same token, whenever inefficient quenching of excitonic luminescence is observed despite dopant excited states within the gap, the cause is likely related to poor dopant–exciton spatial overlap, which can only result from the dopants not being truly incorporated within the QD cores. A situation of this type was recently described in colloidal CdSe/Co^{2+}:CdS core/shell nanocrystals [51]. Overall, the PL of colloidal doped nanocrystals

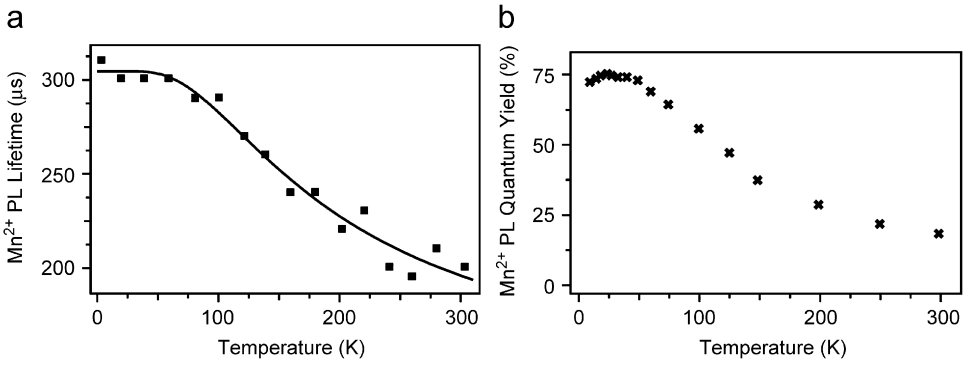

Fig. 3. (a) Temperature dependence of the Mn^{2+} $^4T_1 \rightarrow {}^6A_1$ photoluminescence lifetime in 0.2% Mn^{2+}:ZnSe nanocrystals ($d = 3$–4 nm). The solid line shows a fit of the data to a temperature-activated nonradiative quenching model. Data adapted from Ref. [4]. (b) Temperature dependence of the Mn^{2+} $^4T_1 \rightarrow {}^6A_1$ photoluminescence quantum yield in $d = 2.85$ nm Mn^{2+}:ZnSe nanocrystals made from solution containing 6.3% Mn^{2+} cation concentration. Data adapted from Ref. [7].

described by scenario I are thus primarily limited to applications where excitonic emission is not needed.

In the Mn^{2+}:ZnSe nanocrystals of Fig. 2, Mn^{2+} $^4T_1 \rightarrow {}^6A_1$ PL decay lifetimes of 200–300 μs have been measured for 0.2% Mn^{2+} as a function of sample temperature [4]. These lifetimes show a dependence on temperature that is typical of thermally activated nonradiative relaxation (Fig. 3a), with decreasing lifetimes and PL intensities at increasing temperatures. This behavior most likely involves energy transfer to traps. Even inefficient nonradiative processes can reduce Mn^{2+} PL lifetimes (Fig. 3a) and hence quantum yields (Fig. 3b) substantially because of the very small Mn^{2+} radiative transition rate constants. Overall, nearly quantitative energy transfer from the excited semiconductor to the Mn^{2+} ($k_{ET}^{Mn^{2+}} \gg 0$) results in room-temperature PL quantum yields of Mn^{2+}-doped II–VI nanocrystals that are routinely around 10% and can exceed 50% with additional refinement [19]. The high efficiency of Mn^{2+} PL sensitization by host semiconductor nanocrystals has helped to attract attention to such nanocrystals (scenario I) as colloidal phosphors for bio-imaging applications [18,19] and as recombination centers in light-emitting devices [20,21].

2.2. Scenario II: Mn^{2+} photoionization excited states are lowest in energy and within the gap

A rarer scenario occurs in wide-gap semiconductors, where the existence of donor- or acceptor-type photoionization states within the gap can introduce nonradiative relaxation pathways that largely or entirely quench the nanocrystal emission. For most Mn^{2+}-doped II–VI semiconductors, such as those described by scenario I above, all donor- and acceptor-type photoionization states appear to reside outside of the gap, where they have not been detected because they are obscured by the more intense host semiconductor absorption features. Among Mn^{2+}-doped II–VI semiconductors, the presence of such levels within the gap appears to occur only for Mn^{2+}:ZnO, but it may be more commonly observed when other dopants are used, or for cases of aliovalent doping. For colloidal Mn^{2+}-doped ZnO QDs [52], a sub-bandgap donor-type photoionization state is responsible for this scenario [52,53]. Fig. 4 shows room-temperature absorption and PL spectra of $d \approx 6.0$ nm ZnO, 0.13% Mn^{2+}:ZnO, and 1.3% Mn^{2+}:ZnO colloidal QDs capped with dodecylamine and suspended in toluene. The pure ZnO nanocrystals show the characteristic broad visible trap emission centered at ~18,600 cm^{-1} in addition to near-edge UV emission at 26,900 cm^{-1}. These two features in undoped ZnO nanocrystals have been described in detail previously [54]. The 0.13% Mn^{2+}:ZnO colloids show a similar PL spectrum but the visible and UV emission intensities have been

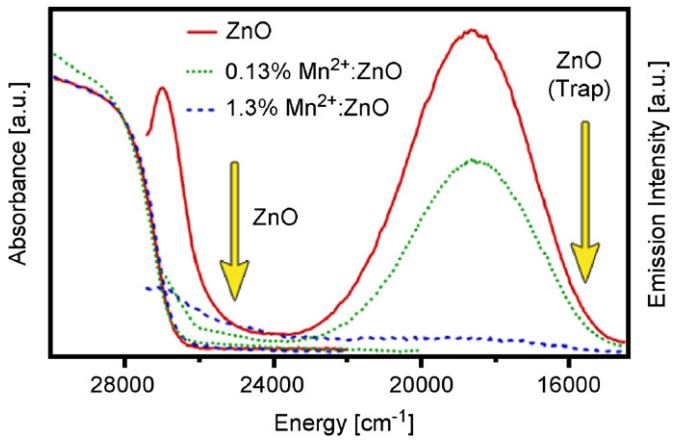

Fig. 4. 300 K absorption and photoluminescence spectra of colloidal ZnO (—), 0.13% Mn^{2+}:ZnO (· · ·), and 1.3% Mn^{2+}:ZnO (- - -) nanocrystals, all with $d \approx 6.0$ nm. The excitonic and visible trap photoluminescence intensities of the undoped ZnO QDs are both quenched upon doping with Mn^{2+}. EPR spectroscopy verifies exclusively substitutional Mn^{2+} doping with no surface Mn^{2+}. Data adapted from Ref. [52].

reduced by roughly 50% relative to the undoped ZnO nanocrystals. In 1.3% Mn^{2+}:ZnO nanocrystals, both PL features are quenched by at least ~95%. In contrast with the Mn^{2+}:ZnSe (Fig. 2) and the other II–VI QDs described by scenario I above, this quenching is not accompanied by appearance of Mn^{2+} $^4T_1 \rightarrow {}^6A_1$ luminescence. To date, Mn^{2+} $^4T_1 \rightarrow {}^6A_1$ emission has not been observed in Mn^{2+}:ZnO QDs. The PL attributed to the Mn^{2+} $^4T_1 \rightarrow {}^6A_1$ ligand-field transition in nanocrystalline Mn^{2+}:ZnO powders [55] is indistinguishable from the visible surface trap emission, and it is likely that this is not Mn^{2+} ligand-field emission. An interesting manganese-related PL signal has recently been reported for 5% Mn^{2+}-doped ZnO thin films (maximum intensity at ~2.06 eV (16,700 cm^{-1}), electronic origin at ~2.5 eV (20,200 cm^{-1}), and multiexponential PL decay with ~>100 μs at 10 K) that was attributed to Mn^{2+} $^4T_1 \rightarrow {}^6A_1$ emission [56]. Further studies of this interesting PL signal should be undertaken to verify its assignment.

The quenching of ZnO QD PL upon Mn^{2+} doping is due to the presence of a sub-bandgap photoionization state. This state is seen in the electronic absorption and magnetic circular dichroism (MCD) spectra of colloidal Mn^{2+}:ZnO QDs (Fig. 5), which both show a broad and intense absorption band extending well below the ZnO band edge. Although often assigned to Mn^{2+} *d–d* transitions [57,58] or Mn_xO_y impurity phases [59], this band has a per-Mn^{2+} molar extinction coefficient of $\varepsilon_{Mn^{2+}} = 950\ M^{-1}\ cm^{-1}$

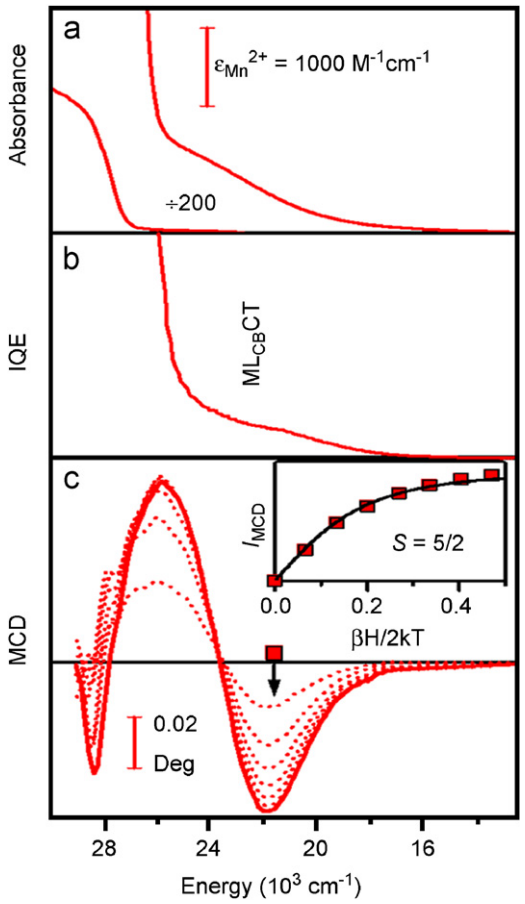

Fig. 5. (a) 300 K absorption spectrum of colloidal TOPO-capped 1.1% Mn^{2+}:ZnO nanocrystals. (b) Photocurrent internal quantum efficiency for charge separation in Mn^{2+}:ZnO nanocrystalline photoanode. (c) Variable-field 5 K MCD spectra of the same nanocrystals as in (a). The inset shows that the broad sub-bandgap MCD intensity follows $S = 5/2$ saturation magnetization and is therefore associated with isolated paramagnetic Mn^{2+} ions. Data adapted from Ref. [53].

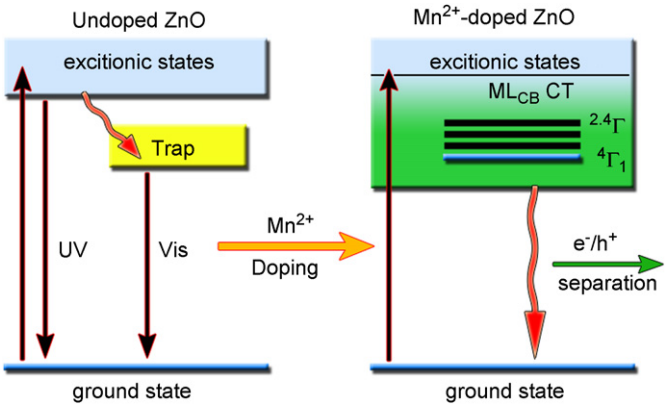

Fig. 6. Effect of Mn^{2+} doping on the photophysical properties of ZnO nanocrystals. The UV and visible (trap) luminescence of ZnO nanocrystals are both quenched, no Mn^{2+} ligand-field photoluminescence is observed, and photo-induced charge separation is observed with sub-bandgap photoexcitation.

at 24,000 cm^{-1} at 300 K [52] that is approximately two orders of magnitude larger than could be reasonably expected for the anticipated Mn^{2+} ligand-field transitions (for example, $\varepsilon_{Mn^{2+}}$ ($^6A_1 \rightarrow {}^4T_1$) = 1–10 M^{-1} cm^{-1} in tetrahedral coordination complexes [60] and in ZnS [43]), and it shows $S = 5/2$ saturation magnetization by MCD, confirming its association with isolated paramagnetic Mn^{2+} ions. Using the Tanabe–Sugano matrices and empirical ligand-field parameters, the $^6A_1 \rightarrow {}^4T_1(G)$, $^4T_2(G)$, $^4A_1(G)$, $^4E(G)$ series of Mn^{2+} ligand-field excited states has been calculated to occur at energies starting at ~24,900 cm^{-1} in ZnO [52], but the 5 K MCD spectrum in this region is structureless (Fig. 1), in contrast with what would be observed were this intensity to arise from this set of ligand-field transitions. This transition has instead been assigned as a donor-type photoionization transition ($Mn^{2+} \rightarrow Mn^{3+}+e^-_{CB}$, or $ML_{CB}CT$) of Mn^{2+}:ZnO on the basis of optical electronegativity considerations [52], and the ligand-field transitions are likely obscured by this band because of the 10^2–10^3 difference in extinction coefficients. This charge-transfer excited state configuration is formally equivalent to a hole-trapped exciton and is related to proposed [61] Zhang–Rice-like states in *p*-type Mn^{2+}:ZnO. Because this photoionization state is the lowest energy excited state, it largely defines the photophysical properties of Mn^{2+}:ZnO nanocrystals. Specifically, it provides an efficient pathway for nonradiative relaxation back to the ground state, as summarized in Fig. 6. The details of this nonradiative relaxation are not yet understood, but multiphonon relaxation often makes the greatest contribution to the overall nonradiative relaxation rate constant. The combination of electron–phonon coupling due to the charge-transfer nature of this excited state, combined with the exponential dependence of multiphonon relaxation rate constants on excited state distortion, make multiphonon relaxation a plausible pathway. An alternative pathway might involve electron trapping from this charge-transfer state, but this is considered less likely because of the experimental ability to introduce additional conduction-band electrons into Mn^{2+}:ZnO nanocrystals without such electron trapping [27]. It is noteworthy that this charge-transfer state is also responsible for the photo-induced charge separation detected at sub-bandgap excitation energies in Mn^{2+}:ZnO photoelectrodes (Fig. 5b) [53]. The appearance of a photoionization state as the lowest energy excited state within the semiconductor bandgap thus makes the electronic structure and photophysical properties of Mn^{2+}:ZnO nanocrystals qualitatively different from those described by scenario I above.

2.3. *Scenario III: semiconductor excitonic excited states are lowest in energy (Mn^{2+} excited states are outside the gap)*

A third distinct scenario can be identified as occurring when no impurity states exist within the gap of the host semiconductor. In some regards this third scenario is the most interesting and fundamentally important, because the size-tunable emission, lasing capabilities, and other photophysical properties that have attracted attention to colloidal undoped semiconductor QDs can be retained, while the Mn^{2+} impurities introduce an additional degree of freedom for controlling these physical properties. Although many syntheses have been attempted, only recently was the first unambiguous experimental demonstration of scenario III colloidal doped semiconductor nanocrystal luminescence reported. These observations were made for colloidal Mn^{2+}:CdSe QDs [62].

The colloidal Mn^{2+}:CdSe QDs differ from all other colloidal doped semiconductor nanocrystals reported to date in that they are the first that have allowed tuning of the semiconductor band gap energy across the dopant excited state levels. Fig. 7 presents PL spectra of small ($d \approx 2.5$ nm) and large ($d \approx 4.2$ nm) Mn^{2+}:CdSe QDs. The characteristic Mn^{2+} $^4T_1$ emission is observed when the bandgap energy is greater than the Mn^{2+} $^4T_1$ excited state energy, but only excitonic emission is observed when the bandgap energy is reduced to below the $^4T_1$ energy in larger Mn^{2+}:CdSe QDs [62]. The excitonic emission observed in the small Mn^{2+}:CdSe nanocrystal sample arises predominantly from undoped nanocrystals,

which occur with greater probability as the nanocrystal diameter is reduced because of dopant exclusion from critical nuclei [13,15,38,39].

Fig. 8 plots the energies of the Mn^{2+} and excitonic PL maxima as a function of nanocrystal diameter for a series of Mn^{2+}:CdSe QDs. The energy of the excitonic transition depends strongly on particle size, but the energy of the localized Mn^{2+} transition does not. The nature of the emissive state changes at $d \approx 3.3$ nm, marking the cross-over between scenarios I and III. Although scenarios I and III both also exist among bulk DMSs, these colloidal Mn^{2+}:CdSe QDs are unique in that they allow tuning from one scenario to the other quite readily, simply by changing the nanocrystal diameter.

Although only excitonic emission is observed in the large Mn^{2+}:CdSe QDs, the properties of this luminescence are still fundamentally altered by the presence of the Mn^{2+} ions. Specifically, the excitonic emission of Mn^{2+}:CdSe QDs with $d > \sim 3.3$ nm can be made strongly circularly polarized by application of a magnetic field, even when the QDs are excited with incoherent or unpolarized photons. This has recently been demonstrated for the first time for any colloidal nanocrystal using magnetic circularly polarized luminescence (MCPL) spectroscopy [62]. MCPL spectroscopy was applied to probe the giant excitonic Zeeman splittings in colloidal Mn^{2+}:CdSe QDs. In the absence of magnetic dopants, the excitonic Zeeman splitting in CdSe QDs is small, linear in magnetic field, and comparable in magnitude to the thermal energy available at a few Kelvins (g_{eff}(CdSe) ≈ +1.5) [63]. Introduction of Mn^{2+} dopants gives rise to strong Mn^{2+}-carrier magnetic exchange coupling, which leads to the so-called "giant excitonic Zeeman splitting" [64]. In its simplest manifestation, the exchange contribution to the excitonic Zeeman splitting energy is described by [16,65–67]

$$\Delta E_{Zeeman}^{exch} = x\langle S_z\rangle N_0(\alpha - \beta) \quad (1)$$

where x is the paramagnetic dopant mole fraction, $\langle S_z \rangle$ is the temperature- and field-dependent spin polarization of the paramagnetic ensemble of dopants along the direction of the applied field, and $N_0(\alpha-\beta)$ describes the strength of the magnetic exchange interactions between the dopants and the charge carriers of the exciton. Typical values for $N_0(\alpha-\beta)$ in both bulk and nanocrystalline Mn^{2+}:CdSe are around +1.5 eV [64,65], leading to effective Zeeman splittings that are at least one to two orders of magnitude larger for Mn^{2+}:CdSe QDs than for undoped CdSe QDs. Furthermore, because Mn^{2+} spin expectation values oppose the direction of the applied field (ie. $\langle S_z \rangle < 0$) [68], these exchange-induced Zeeman splittings oppose the small intrinsic Zeeman splitting of undoped CdSe QDs. The result is an inversion of the excitonic Zeeman splittings upon Mn^{2+} doping, which is most readily observed as an inversion in the circular polarization of the excitonic emission. Experimental results are summarized in Fig. 9, which plots the luminescence polarization ratio $\Delta I/I = (I_L - I_R)/(I_L + I_R)$ as a function of applied magnetic field for $d \approx 4$ nm CdSe and Mn^{2+}:CdSe quantum dots. Here, I_L and I_R refer to the intensities of left- and right-circularly polarized luminescence, respectively, following the sign convention of Piepho and Schatz [69]. The sign inversion and large increase in MCPL polarization ratio observed upon doping derive from the giant excitonic Zeeman splitting in the Mn^{2+}:CdSe QDs. Similar results were also observed by MCD spectroscopy for the same colloidal Mn^{2+}:CdSe nanocrystals [16,62].

Reducing the energy gap of the host semiconductor to below all Mn^{2+} excited state energies by quantum confinement tuning thus completely alters the photophysical properties of colloidal doped semiconductor nanocrystals, and yields a new scenario (scenario III) that is fundamentally different from the two described above (scenarios I and II). With the new possibility to control the excitonic PL of colloidal QDs using magnetism, one can now envision practical routes to systematic examination of the

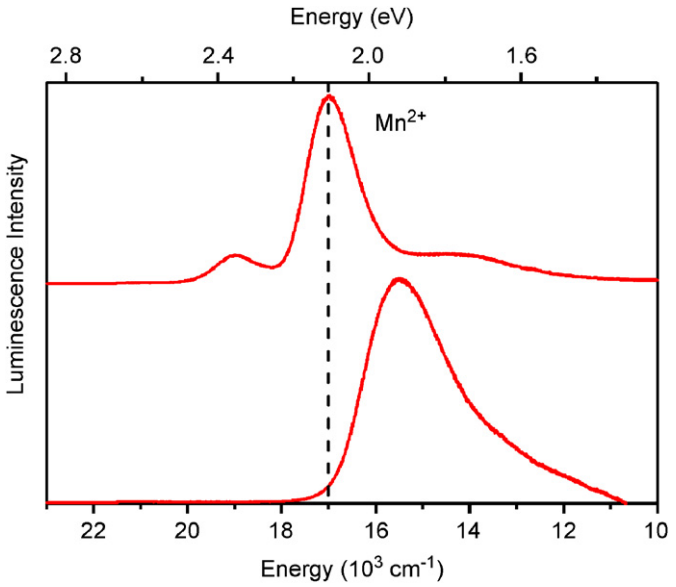

Fig. 7. Low-temperature (5 K) photoluminescence spectra of colloidal $d \approx 2.5$ nm (top) and $d \approx 4.2$ nm (bottom) Mn^{2+}:CdSe quantum dots. The vertical dotted line marks the energy of the Mn^{2+} $^4T_1 \rightarrow {}^6A_1$ luminescence maximum (2.11 eV), which is observed only in small Mn^{2+}:CdSe QDs. Adapted from Ref. [62].

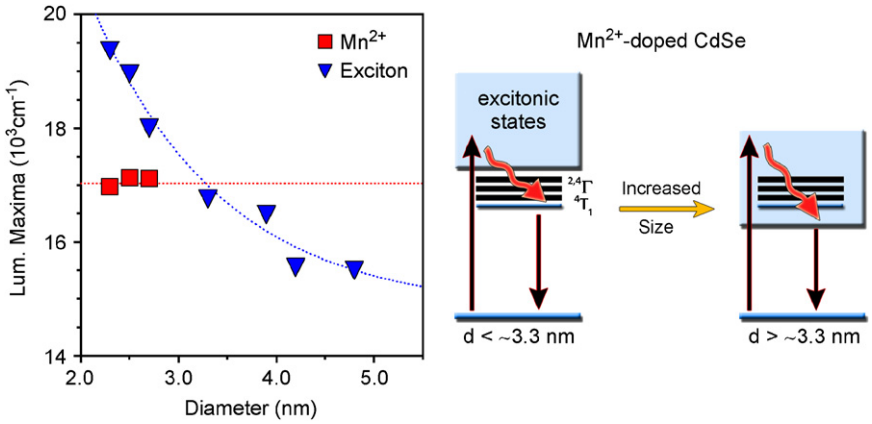

Fig. 8. Energies of the Mn^{2+} $^4T_1$ and CdSe excitonic photoluminescence maxima plotted vs. Mn^{2+}:CdSe nanocrystal diameter. The two features cross at $d \approx 3.3$ nm. Adapted from Ref. [62].

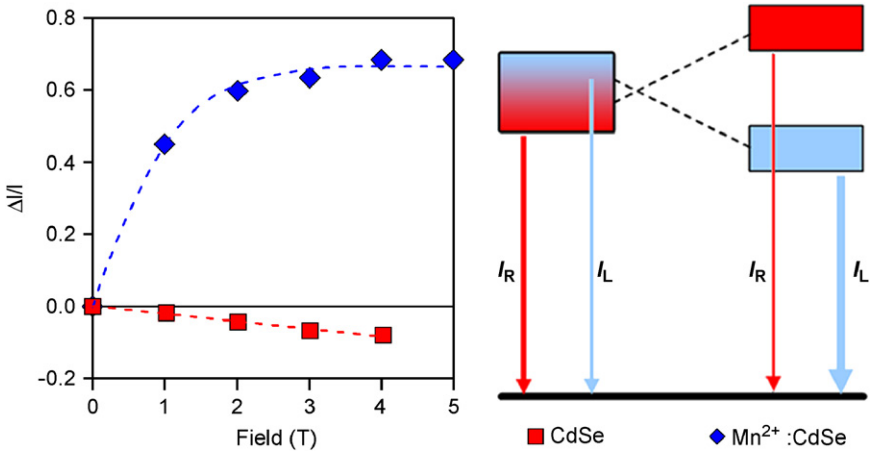

Fig. 9. Left: excitonic MCPL polarization ratios for $d \approx 4.2$ nm 4.5% Mn^{2+}:CdSe (◆) and $d \approx 4.0$ nm CdSe (■) QDs as a function of magnetic field. The sign inversion and saturation with magnetic field observed for the Mn^{2+}:CdSe QDs are signatures of the giant excitonic Zeeman splitting. Right: schematic illustration of the sign inversion and enhancement of the excitonic Zeeman splittings upon doping for a fixed magnetic field strength. Data adapted from Ref. [62].

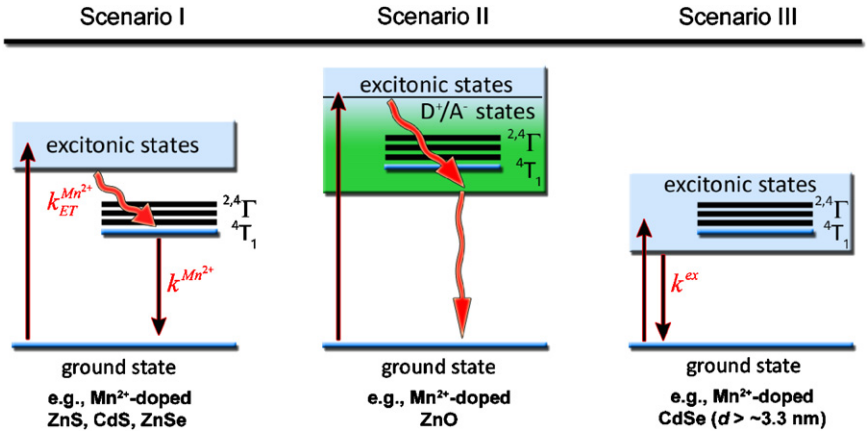

Fig. 10. Schematic summary of the different electronic structures related to photoluminescence observed in colloidal Mn^{2+}-doped semiconductor nanocrystals described in the case studies above. Radiative processes are indicated by straight arrows, and nonradiative processes by curved arrows. In scenario I, efficient energy transfer ($k_{ET}^{Mn^{2+}}$) quenches excitonic emission and sensitizes Mn^{2+} $^4T_1 \rightarrow {}^6A_1$ luminescence. In scenario II, excitons are quenched by Mn^{2+} photoionization states (dopant-bound excitons) that relax nonradiatively to the ground state. In scenario III, all Mn^{2+} excited states are outside of the semiconductor band gap, and the nanocrystals show excitonic emission. Examples of Mn^{2+}-doped II–VI DMS nanocrystals of each type are provided. For clarity, relaxation processes involving other surface or lattice defects are not depicted. Figure adapted from Ref. [62].

importance of energy gaps in energy transfer dynamics and magnetic exchange coupling for the first time using PL and magneto-PL spectroscopies. A great number of interesting new experiments and discoveries can be anticipated involving this new type of colloidal doped QDs.

3. Overview and outlook

Fig. 10 summarizes schematically the electronic structural features of colloidal Mn^{2+}-doped II–VI semiconductor nanocrystals that lead to the three distinct photophysical scenarios described above. These three scenarios reflect three distinct relationships between the energies of the magnetic ions' excited states and those of the host semiconductor nanocrystals. Scenario III PL has only very recently been demonstrated, in Mn^{2+}-doped CdSe semiconductor nanocrystals [62]. In that case, the size dependence of the excitonic energies allowed tuning between scenarios I and III simply by changing the Mn^{2+}:CdSe nanocrystal diameter.

The three scenarios summarized in Fig. 10 apply generally as limiting cases for this entire class of materials, including bulk DMSs. Variations on these three scenarios can also be anticipated in intermediate cases for which electronic structures approach cross-over points between these three limiting scenarios or when other dopants are used. A widely studied example is Co^{2+}, which has been doped into colloidal II–VI nanocrystals of ZnO [13,70,71], ZnS [40], CdS [40,72], ZnSe [15,17,24], and CdSe [16,24,51], and for which nonradiative relaxation within the manifold of ligand-field excited states is more important than for Mn^{2+}. Finally, the PL phenomena described in this short review have been limited to only the most basic materials, those in which Mn^{2+} is simply substituted into binary II–VI semiconductor nanocrystals. Rich photophysical effects can be anticipated as synthetic efforts are extended to address doped colloidal core/shell nanocrystals [18,25,26,51] anisotropic nanostructures [73–75] and hetero-architectures or superlattices integrating doped nanocrystals with other functional inorganic or organic materials. Future experiments in these directions may ultimately lead to fine synthetic control over dopant-exciton spatial overlap, a deeper understanding of the influences of dopant concentrations and

distributions within QDs, and ultimately to new nanoscale materials with chemically controlled magneto-electronic, magneto-photonic, photochemical, or photoluminescent properties for future applications in nanotechnology.

Acknowledgments

The authors thank their coworkers, collaborators and collegues who have contributed to research described in this manuscript, including: X. Liu, S. Lee, G.M. Salley, M. Dobrowolska, J.K. Furdyna, A. Meijerink, J. van Rijssel, W.K. Liu, S.A. Santangelo, N.S. Norberg, and K.R. Kittilstved. Financial support from the US NSF (PECASE DMR-0239325 to D.G.), Research Corporation, Dreyfus Foundation, Sloan Foundation, and the NSERC Postdoctoral Fellowship program (to R.B.) is gratefully acknowledged.

References

[1] W. Chen, J.Z. Zhang, A.G. Joly, Optical properties and potential applications of doped semiconductor nanoparticles, J. Nanosci. Nanotech. 4 (2004) 919–947.
[2] H. Yang, S. Santra, P.H. Holloway, Syntheses and applications of Mn-doped II–VI semiconductor nanocrystals, J. Nanosci. Nanotech. 5 (2005) 1364–1375.
[3] K. Kanemitsu, A. Ishizumi, Luminescence properties of impurity-doped semiconductor nanoparticles, J. Lumin. 119–120 (2006) 161–166.
[4] J.F. Suyver, S.F. Wuister, J.J. Kelly, A. Meijerink, Luminescence of nanocrystalline ZnSe:Mn^{2+}, Phys. Chem. Chem. Phys. 2 (2000) 5445–5448.
[5] J.F. Suyver, T. van der Beek, S.F. Wuister, J.J. Kelly, A. Meijerink, Luminescence of nanocrystalline ZnSe:Cu, Appl. Phys. Lett. 79 (2001) 4222–4224.
[6] A.A. Bol, A. Meijerink, Long-lived Mn^{2+} emission in nanocrystalline ZnS:Mn^{2+}, Phys. Rev. B 58 (1998) 15997–16000.
[7] D.J. Norris, N. Yao, F.T. Charnock, T.A. Kennedy, High-quality manganese-doped ZnSe nanocrystals, Nano Lett. 1 (2001) 3–7.
[8] N. Pradhan, X. Peng, Efficient and color-tunable Mn-doped ZnSe nanocrystal emitters: control of optical performance via greener synthetic chemistry, J. Am. Chem. Soc. 129 (2007) 3339–3347.
[9] A.A. Bol, R. van Beek, J. Ferwerda, A. Meijerink, Temperature dependence of the luminescence of nanocrystalline CdS/Mn^{2+}, J. Phys. Chem. Solids 64 (2003) 247–252.
[10] L. Chen, F.J. Brieler, M. Fröba, P.J. Klar, W. Heimbrodt, Quantitative description of the temporal behavior of the internal Mn $3d^5$ luminescence in ensembles of $Zn_{0.99}Mn_{0.01}S$ quantum dots, Phys. Rev. B 75 (2007) 241303(R).
[11] M.A. Chamarro, V. Voliotis, R. Grousson, P. Lavallard, T. Gacoin, G. Counio, J.P. Boilot, R. Cases, Optical properties of Mn-doped CdS nanocrystals, J. Cryst. Growth 159 (1996) 853–856.
[12] D.M. Hoffman, B.K. Meyer, A.I. Ekimov, I.A. Merkulov, A.L. Efros, M. Rosen, G. Counio, T. Gacoin, J.-P. Boilot, Giant internal magnetic fields in Mn doped nanocrystal quantum dots, Solid State Commun. 114 (2000) 547–550.
[13] D.A. Schwartz, N.S. Norberg, Q.P. Nguyen, J.M. Parker, D.R. Gamelin, Magnetic quantum dots: synthesis, spectroscopy, and magnetism of Co^{2+}- and Ni^{2+}-doped ZnO nanocrystals, J. Am. Chem. Soc. 125 (2003) 13205–13218.
[14] N.S. Norberg, D.R. Gamelin, Giant Zeeman effects in colloidal diluted magnetic semiconductor quantum dots with homogeneous dopant speciation, J. Appl. Phys. 99 (2005) 08M104.
[15] N.S. Norberg, G.L. Parks, G.M. Salley, D.R. Gamelin, Giant excitonic Zeeman splittings in Co^{2+}-doped ZnSe quantum dots, J. Am. Chem. Soc. 128 (2006) 13195–13203.
[16] P.I. Archer, S.A. Santangelo, D.R. Gamelin, Direct observation of sp–d exchange interactions in colloidal Mn^{2+}- and Co^{2+}-doped CdSe quantum dots, Nano Lett. 7 (2007) 1037–1043.
[17] N.S. Norberg, G.M. Dalpian, J.R. Chelikowsky, D.R. Gamelin, Energetic pinning of magnetic impurity levels in quantum confined semiconductor nanocrystals, Nano Lett. 6 (2006) 2887–2892.
[18] S. Wang, B.R. Jarrett, S.M. Kauzlarich, A.Y. Louie, Core/shell quantum dots with high relaxivity and photoluminescence for multimodality imaging, J. Am. Chem. Soc. 129 (2007) 3848–3856.
[19] N. Pradhan, D.M. Battaglia, Y. Liu, X. Peng, Efficient, stable, small, and water-soluble doped ZnSe nanocrystal emitters as non-cadmium biomedical labels, Nano Lett. 7 (2007) 312–317.
[20] H. Yang, P.H. Holloway, Electroluminescence from hybrid conjugated polymer-CdS:Mn/ZnS core/shell nanocrystals devices, J. Phys. Chem. B 107 (2003) 9705–9710.
[21] H. Yang, P.H. Holloway, B.B. Ratna, Photoluminescent and electroluminescent properties of Mn-doped ZnS nanocrystals, J. Appl. Phys. 93 (1) (2003) 586–592.
[22] A.L. Efros, E.I. Rashba, M. Rosen, Paramagnetic ion-doped nanocrystal as a voltage-controlled spin filter, Phys. Rev. Lett. 87 (2001) 206601.
[23] R.M. Abolfath, P. Hawrylak, I. Zutic, Electronic states of magnetic quantum dots, New J. Phys. 9 (2007) 353.
[24] S.A. Santangelo, E.A. Hinds, V.A. Vlaskin, P.I. Archer, D.R. Gamelin, Bimodal bond-length distributions in cobalt-doped CdSe, ZnSe, and $Cd_{1-x}Zn_xSe$ quantum dots, J. Am. Chem. Soc. 129 (2007) 3973–3978.
[25] Y. Yang, O. Chen, A. Angerhofer, Y.C. Cao, Radial-position-controlled doping in CdS/ZnS core/shell nanocrystals, J. Am. Chem. Soc. 128 (2006) 12428–12429.
[26] S. Ithurria, P. Guyot-Sionnest, B. Mahler, B. Dubertret, Mn^{2+} as a radial pressure gauge in colloidal core/shell nanocrystals, Phys. Rev. Lett. 99 (2007) 265501.
[27] W.K. Liu, K.M. Whitaker, K.R. Kittilstved, D.R. Gamelin, Stable photogenerated carriers in magnetic semiconductor nanocrystals, J. Am. Chem. Soc. 128 (2006) 3910–3911.
[28] J. Fernández-Rossier, R. Aguado, Mn-doped II–VI quantum dots: artificial molecular magnets, Phys. Status Solidi (c) 3 (2006) 3734–3739.
[29] F. Qu, P. Hawrylak, Magnetic exchange interactions in quantum dots containing electrons and magnetic ions, Phys. Rev. Lett. 95 (2005) 217206.
[30] F. Qu, P. Hawrylak, Theory of electron mediated Mn–Mn interactions in quantum dots, Phys. Rev. Lett. 96 (2006) 157201.
[31] A.O. Govorov, Voltage-tunable ferromagnetism in semimagnetic quantum dots with few particles: magnetic polarons and electrical capacitance, Phys. Rev. B 72 (2005) 075359.
[32] P.V. Radovanovic, D.R. Gamelin, High-temperature ferromagnetism in Ni^{2+}-doped ZnO aggregates prepared from colloidal diluted magnetic semiconductor quantum dots, Phys. Rev. Lett. 91 (2003) 157202.
[33] P.I. Archer, P.V. Radovanovic, S.M. Heald, D.R. Gamelin, Low-temperature activation and deactivation of high-T_C ferromagnetism in a new diluted magnetic semiconductor: Ni^{2+}-doped SnO_2, J. Am. Chem. Soc. 127 (2005) 14479–14487.
[34] P.I. Archer, D.R. Gamelin, Controlled grain boundary defect formation and its role in the high-T_C ferromagnetism of Ni^{2+}:SnO_2, J. Appl. Phys. 99 (2006) 08M107.
[35] P.I. Archer, D.R. Gamelin, Chemical approaches using nanocrystals to control lattice defect formation and explore the high-T_C ferromagnetism of oxide diluted magnetic semiconductors, in: N.H. Hong (Ed.), Magnetism in Semiconducting Oxides, Research Signpost, Trivandrum, India, 2007.
[36] J.D. Bryan, S.M. Heald, S.A. Chambers, D.R. Gamelin, Strong room-temperature ferromagnetism in Co^{2+}-doped TiO_2 made from colloidal nanocrystals, J. Am. Chem. Soc. 126 (2004) 11640–11647.
[37] J.D. Bryan, S.A. Santangelo, S.C. Keveren, D.R. Gamelin, Activation of high-T_C ferromagnetism in Co^{2+}:TiO_2 and Cr^{3+}:TiO_2 nanorods and nanocrystals by grain boundary defects, J. Am. Chem. Soc. 127 (2005) 15568–15574.
[38] J.D. Bryan, D.R. Gamelin, Doped semiconductor nanocrystals: synthesis, characterization, physical properties, and applications, Prog. Inorg. Chem. 54 (2005) 47–126.
[39] J.D. Bryan, D.A. Schwartz, D.R. Gamelin, The influence of dopants on the nucleation of semiconductor nanocrystals from homogeneous solution, J. Nanosci. Nanotech. 5 (2005) 1472–1479.
[40] P.V. Radovanovic, D.R. Gamelin, Electronic absorption spectroscopy of cobalt ions in diluted magnetic semiconductor quantum dots: demonstration of an isocrystalline core/shell synthetic method, J. Am. Chem. Soc. 123 (2001) 12207–12214.
[41] S.C. Erwin, L.J. Zu, M.I. Haftel, A.L. Efros, T.A. Kennedy, D.J. Norris, Doping semiconductor nanocrystals, Nature 436 (2005) 91–94.
[42] W. Chen, A Special Issue on Doped Nanomaterials, J. Nanosci. Nanotech 5 (2005) i–iii and references therein.
[43] J. Dreyhsig, J.W. Allen, Absorption from the excited state in ZnS:Mn, J. Phys.: Condens. Matter 1 (1989) 1087–1099.
[44] W.W. Yu, L. Qu, W. Guo, X. Peng, Experimental determination of the extinction coefficient of CdTe, CdSe and CdS, Chem. Mater. 15 (14) (2003) 2854–2860.
[45] W.W. Yu, L. Qu, W. Guo, X. Peng, Experimental determination of the extinction coefficient of CdTe, CdSe and CdS, Chem. Mater. 16 (3) (2004) 560 (Erratum).
[46] H.-E. Gümlich, Electro- and photoluminescence properties of Mn^{2+} in ZnS and ZnCdS, J. Lumin. 23 (1981) 73–99.
[47] T.J. Norman, D. Magana, T. Wilson, C. Burns, J.Z. Zhang, Optical and surface structural properties of Mn^{2+}-doped ZnSe nanoparticles, J. Phys. Chem. B 107 (2003) 6309–6317.
[48] J.H. Chung, C.S. Ah, D.-J. Jang, Formation and distinctive decay times of surface- and lattice-bound Mn^{2+} impurity luminescence in ZnS nanoparticles, J. Phys. Chem. B 105 (2001) 4128–4132.
[49] J. Seufert, G. Bacher, M. Scheibner, A. Forchel, S. Lee, M. Dobrowolska, J.K. Furdyna, Dynamical spin response in semimagnetic quantum dots, Phys. Rev. Lett. 88 (2002) 027402.
[50] D.L. Dexter, A theory of sensitized luminescence in solids, J. Chem. Phys. 21 (1953) 836–850.
[51] P.I. Archer, S.A. Santangelo, D.R. Gamelin, Inorganic cluster syntheses of TM^{2+}-doped quantum dots (CdSe, CdS, CdSe/CdS): physical property dependence on dopant locale, J. Am. Chem. Soc. 129 (2007) 9808–9818.
[52] N.S. Norberg, K.R. Kittilstved, J.E. Amonette, R.K. Kukkadapu, D.A. Schwartz, D.R. Gamelin, Synthesis of colloidal Mn^{2+}:ZnO quantum dots and high-T_C ferromagnetic nanocrystalline thin films, J. Am. Chem. Soc. 126 (2004) 9387–9398.
[53] K.R. Kittilstved, W.K. Liu, D.R. Gamelin, Electronic structure origins of polarity dependent high-T_C ferromagnetism in oxide diluted magnetic semiconductors, Nat. Mater. 5 (2006) 291–297.

[54] A. van Dijken, E.A. Meulenkamp, D. Vanmaekelbergh, A. Meijerink, Identification of the transition responsible for the visible emission in ZnO using quantum size effects, J. Lumin. 90 (2000) 123–128.
[55] R.N. Bhargava, T.S. Chhabra, A. Ekimov, N. Taskar, Quantum confined atoms of doped ZnO nanocrystals, Phys. Status Solidi (b) 229 (2002) 897–901.
[56] M. Nakayama, H. Tanaka, K. Masuko, T. Fukushima, A. Ashida, N. Fujimura, Photoluminescence properties peculiar to the Mn-related transition in a lightly alloyed ZnMnO thin film grown by pulsed laser deposition, Appl. Phys. Lett. 88 (2006) 241908.
[57] Y.S. Wang, P.J. Thomas, P. O'Brien, Optical properties of ZnO nanocrystals doped with Cd, Mg, Mn, and Fe ions, J. Phys. Chem. B 110 (2006) 21412–21415.
[58] Z.-W. Jin, Y.-Z. Yoo, T. Sekiguchi, T. Chikyow, H. Ofuchi, H. Fujioka, M. Oshima, H. Koinuma, Blue and ultraviolet cathodoluminescence from Mn-doped epitaxial ZnO thin films, Appl. Phys. Lett. 83 (2003) 39–41.
[59] J.R. Neal, A.J. Behan, R.M. Ibrahim, H.J. Blythe, M. Ziese, A.M. Fox, G. Gehring, Room-temperature magneto-optics of ferromagnetic transition-metal-doped ZnO thin films, Phys. Rev. Lett. 96 (2006) 197208.
[60] A.B.P. Lever, Inorganic Electronic Spectroscopy, second ed, Elsevier Science Publishers, Amsterdam, 1984.
[61] T. Dietl, Hole states in wide band-gap diluted magnetic semiconductors and oxides, Phys. Rev. B. 77 (2007) 085208.
[62] R. Beaulac, P.I. Archer, X. Liu, S. Lee, G.M. Salley, M. Dobrowolska, J.K. Furdyna, D.R. Gamelin, Spin-polarizable excitonic luminescence in colloidal Mn^{2+}-doped CdSe quantum dots, Nano Lett. 8 (2008) 1197–1201.
[63] M. Kuno, M. Nirmal, M.G. Bawendi, A. Efros, M. Rosen, Magnetic circular dichroism study of CdSe quantum dots, J. Chem. Phys. 108 (1998) 4242–4247.
[64] J.K. Furdyna, J. Kossut, Diluted Magnetic Semiconductors, vol. 25, Academic, New York, 1988.
[65] A. Hundt, J. Puls, F. Henneberger, Spin properties of self-organized diluted magnetic $Cd_{1-x}Mn_xSe$ quantum dots, Phys. Rev. B 69 (2004) 121309(R).
[66] G. Bacher, Optical spectroscopy on epitaxially grown II–VI single quantum dots, Top. Appl. Phys. 90 (2003) 147–185 (review).
[67] T. Schmidt, M. Scheibner, L. Worschech, A. Forchel, T. Slobodskyy, L.W. Molenkamp, Sign reversal and light controlled tuning of circular polarization in semimagnetic CdMnSe quantum dots, J. Appl. Phys. 100 (2006) 123109.
[68] J.A. Gaj, Magnetooptical properties of large-gap diluted magnetic semiconductors, in: J.K. Furdyna, J. Kossut (Eds.), Semiconductors and Semimetals (Diluted Magnetic Semiconductors), vol. 25, Academic Press, San Diego, 1988, pp. 275–309.
[69] S.B. Piepho, P.N. Schatz, Group Theory in Spectroscopy with Applications to Magnetic Circular Dichroism, Wiley, New York, 1983.
[70] P.V. Radovanovic, N.S. Norberg, K.E. McNally, D.R. Gamelin, Colloidal transition-metal-doped ZnO quantum dots, J. Am. Chem. Soc. 124 (2002) 15192–15193.
[71] P. Lommens, P.F. Smet, C. de Mello Donegá, A. Meijerink, L. Piraux, S. Michotte, S. Mátéfi-Tempfli, D. Poelman, Z. Hens, Photoluminescence properties of Co^{2+}-doped ZnO nanocrystals, J. Lumin. 118 (2006) 245–250.
[72] V. Ladizhansky, S. Vega, Doping of CdS nanoparticles by Co^{2+} ions studied by NMR, J. Phys. Chem. B 104 (2000) 5237–5241.
[73] P.V. Radovanovic, C.J. Barrelet, S. Gradeak, F. Qian, C.M. Lieber, General synthesis of manganese-doped II–VI and III–V semiconductor nanowires, Nano Lett. 5 (2005) 1407–1411.
[74] J.S. Kulkarni, O. Kazakova, J.D. Holmes, Dilute magnetic semiconductor nanowires, Appl. Phys. A 85 (2006) 277–286.
[75] P.V. Radovanovic, K.G. Stamplecoskie, B.G. Pautler, Dopant ion concentration dependence of growth and faceting of manganese-doped GaN nanowires, J. Am. Chem. Soc. 129 (2007) 10980–10981.